Grid Forming Control Tuning for a Hybrid Inverter-Based Resource Power Plant

Lingling Fan, *Fellow, IEEE*, Zhixin Miao, *Senior Member, IEEE*,
Deepak Ramasubramanian, *Senior Member, IEEE*

***Abstract*—A hybrid inverter-based resource (IBR) power plant consists of grid-following (GFL) and grid-forming inverter-based resources (GFM-IBR) connected in parallel. This research focuses on how to design and tune GFM's control parameters to ensure stable operation of the hybrid power plant for weak and strong grid conditions. We consider two design cases: one where the GFL-IBR does not provide frequency support, and one where it does. It is found that the GFM's power-frequency synchronizing system can lose stability when the power-frequency droop constant is large and/or the grid is strong. Additionally, if the GFL has its frequency support enabled, oscillation stability worsens. To explain the mechanism of the interactions, we construct a feedback system for the synchronizing loop, which consists of the GFM's power-frequency droop control that generates the GFM's synchronizing angle, the GFL's phase-locked loop that measures the voltage phase angle, the GFL's frequency-power control that generates its power order, and the rest of the system. The feedback system is effective in illustrating the potential stability risks. Successful design ensures that the hybrid power plant can operate smoothly and ride through grid disturbances.**

***Index Terms*—Inverter-based resources, grid-following, grid-forming, oscillations, feedback systems.**

I. Introduction

MANY existing IBRs are using legacy grid-following (GFL) control, where a phase-locked loop (PLL) is responsible for synchronization and real/reactive power regulation is achieved through vector current control [1]. On the other hand, to fulfill the requirement of IEEE Standard 2800-2022 [2] for bulk power systems (BPS)-connected IBR power plants, frequency support and voltage support are required. Grid-forming (GFM) control that relies on power-based synchronizing (e.g., [3]) can provide frequency and voltage support. Addition of GFM-IBRs in an IBR power plant may lead to many hybrid power plants with both types of IBRs. This paper investigates how to tune GFM parameters to ensure stable operation of a hybrid power plant for both weak and strong grid conditions. In turn, potential stability issues in a hybrid IBR power plant will also be identified.

A. A brief history of multi-loop GFM and the stability issues

As mentioned by Du *et al.* in [4], two types of P-f droop-based GFM are popular: the single-loop GFM developed by Lasseter for microgrid projects in U.S. [5] and the multi-loop GFM widely adopted in the literature [1], [6], [7]. The multi-loop GFM has inner current control and outer voltage control. Both the inner and outer control loops include cross-coupling and feedforward units.

This type of GFM structure has been examined in the classic book on voltage-sourced converters (VSC) [1] (chapter 9 controlled-frequency VSC system), except that the frequency is assumed to be fixed for autonomous operation. In [1], the control is implemented in the dq frame based on the synchronizing angle, and the voltage control design is derived from the plant model of the filter capacitor dynamics. In a numerical example presented in [1] (Example 9.3), the design leads to a closed-loop control with a bandwidth of 170 Hz.

This multi-loop GFM control structure may be traced back to a 2004 paper by Li *et al.* [6], in which a microgrid consisting of multiple VSCs is studied. The VSC control includes an inner current proportional control and an outer voltage control (also proportional). Both controllers are implemented in the static frame and the voltage-control bandwidth is approximately 2 kHz. The angle and voltage magnitude are generated by the real and reactive power controllers.

In 2007, a multi-loop control scheme in the dq frame was designed by T.C. Green and co-authors [7] for 10-kW 200-V (per phase RMS) inverters. The outer voltage control structure proposed in this paper has since been adopted by many follow-up research, including [1]. In [7], with the filter capacitor size as 50 μF and the proportional-integral (PI) controller of $0.05 + 390/s$, the voltage control achieves a bandwidth of 700 Hz. This is significantly higher than the bandwidth reported in [1]. A quick examination of [4] shows an even higher voltage-control bandwidth at about 4 kHz (using the a 191-μF filter capacitor and a per-unit voltage controller of $10 + 200/s$, with a 100-kW power base and a 480-V voltage base). These inconsistencies make the parameter selection process for voltage controllers rather puzzling.

It is worth noting that the dq-frame voltage control objective—regulating the d-axis voltage to follow a reference and regulating the q-axis voltage to zero—is equivalent to controlling the voltage magnitude through the d-axis while aligning the point of common coupling (PCC) voltage space vector with the synchronous reference frame through the q-axis.

For the multi-loop GFM with coupled voltage control, increasing P-f droop parameters has shown to lead to oscillations in [4], [7] even in the microgrid operation case. For example, Fig. 12 of [7] shows that when the P-f droop parameter

This project is supported in part by US Department of Energy Award DE-EE0011474 and in part by EPRI Grant 10017639. L. Fan and Z. Miao are with the Department of Electrical Engineering, University of South Florida, Tampa, FL, 33620 (e-mail: linglingfan@usf.edu, zmiao@usf.edu). D. Ramasubramanian is with EPRI (email: dramasubramanian@epri.com).

increases to 1.9e-4 rad/(s.W) (or 0.6% pu/pu), the microgrid experiences 10-Hz oscillations. Fig. 7 of [4] shows that when P-f droop parameter increases to 2.3%, the system experiences 20-Hz oscillations. Reported by T.C. Green and co-authors, when this type of GFM is deployed in the grid-connected mode, it is vulnerable for small-signal stability in strong grids [10]. This weak spot was reported by [11] as well.

Therefore, it becomes clear that proper GFM parameter design is crucial for achieving stable operation. This paper focuses on addressing the gap in GFM parameter selection for hybrid power plants, particularly when they operate alongside GFL-IBRs providing frequency support.

B. Literature survey of stability analysis of multiple IBR systems

A few papers are somewhat related to the stability analysis of multiple IBRs and can be grouped into two categories: Category 1 [12], [13] and Category 2 [11], [14], [15]. The first category studies networks with dispersed IBRs to analyze IBR interactions. For example, [12] examined the transient stability for a power grid dominated by different types of GFM-IBRs. Those GFM-IBRs are all equipped with power-based synchronization control in the form of either frequency droop (without inertia) or virtual synchronous machine type of control with the capability to provide inertia. The paper finds that the droop control dramatically enhances the damping effect and the transient stability region.

Reference [13] examines a scenario when a GFL-IBR is sending power to a GFM-IBR. This scenario emulates a wind generator delivering power to an HVDC terminal where the wind generator's interfacing inverter is in GFL control mode while the HVDC's converter is in the GFM control mode. It is found that the system is subject to oscillatory stability issues when the phase-locked loop (PLL) of the GFL has a high bandwidth. This phenomenon is similar to many phenomena observed in GFL grid integration system (e.g., [16]) and it is attributed to GFL's PLL. The topologies in these two papers [12], [13] are for power transfer studies among IBRs. These are very different from our goal of a hybrid power plant interconnected to a main grid or serving loads.

In the second categories, the testbed setup aligns with the hybrid power plant setup. For example, [14] examined the combination of GFL and GFM inverters on transient stability. Simulation studies show that if a GFL is equipped with a voltage to reactive power (current) droop control, the system has better transient stability. The larger the droop control gain, the greater transient stability can be achieved. Another reference [15] focuses on how to yield required the frequency droop slope through GFL and GFM parameterization for a bus connected to both GFL-IBRs and GFM-IBRs.

These two papers have not conducted a thorough examination of small-signal stability of a hybrid power plant.

Reference [11] has used a testbed with two IBRs—one GFL and the other GFM —connected to a grid. Moreover, the control schemes of the GFL and the GFM are similar to those in the current paper. [11] has also found that that "a strong grid with GFM converters and low network impedance is likely to suffer from low-frequency oscillations (e.g., subsynchronous oscillation)."

While the authors of [11] primarily rely on voltage/current relationships or impedance models to build feedback systems, our approach focuses on developng customized feedback systems and providing deeper insights. Additionally, [11] concentrates on identifying stability issues among IBRs and between IBRs and the grid, without considering frequency support through GFL-IBRs. Introducing frequency support via GFL-IBRs increases the coupling between GFL- and GFM-IBRs, necessitating a more detailed analysis. This paper aims to address that gap.

C. Goals and contributions

We will identify potential small-signal stability issues in a hybrid power plant and conduct proper design for GFM. A testbed of a hybrid power plant operating in both the grid-connected mode and the autonomous mode will be constructed in the electromagnetic transient (EMT) simulation environment. EMT simulation will be conducted to identify potential stability issues. Second, once stability issues are identified, this paper adopts design-oriented analysis to examine the mechanism of the identified stability issues.

Design-oriented analysis is a term coined by R. D. Middlebrook. This approach begins with a simple model, such as a block diagram, and incrementally adds details as needed. In essence, design-oriented analysis develops models that are simple yet physically insightful, following a divide-and-conquer methodology [17], [18]. Construction of block diagrams and frequency-domain analysis have long been employed by power system dynamics experts—such as Concordia [[19] and E. V. Larsen [20]—to study the stability of synchronous machines.

In the literature of IBR related stability analysis, this approach has been adopted by several papers [21]–[23] when conducting stability analysis. For example, in [21], the authors examined synchronizing stability of a grid-forming IBR with power-frequency droop and developed a first-order feedback system for characterization. In [22], transient stability or synchronizing stability of a grid-following IBR interconnected to a grid represented by a Thévenin equivalent is characterized through a 2nd-order feedback system by considering PLL's dynamics only. In the authors' upcoming Power & Energy magazine paper [24], many real-world event root cause analysis and replication have been carried out using this approach.

In summary, our unique contribution of this research is three-fold.

- Mechanism analysis on why GFM is vulnerable for stability issues in a strong grid is provided using the power-frequency feedback system and frequency-domain analysis.
- Potential small-signal stability issues, in particular, interactions between GFL-IBRs and GFM-IBRs in a hybrid power plant have been identified and thoroughly analyzed. It is found that equipping GFL-IBR with frequency control may introduce such interactions. A feedback system consisting of both GFL-IBR's and GFM-IBR's

frequency control, as well as the rest of the system has been constructed. This feedback system helps quantitative stability analysis and revealing insights.

- This research leads to a well-coordinated design for GFM in hybrid power plants and enhanced transient stability can be achieved through with GFL's frequency control enabled.

D. Structure of the paper

The rest of the paper is structured as follows. Section II describes the testbed and the control logic. Section III presents the potential small-signal stability issues in strong grids through analysis and EMT demonstration. Section IV presents the benefit of a well-designed GFM operating alongside a GFL with frequency support for transient stability improvement. Finally, section V concludes this paper.

II. A Hybrid Power Plant Test Bed & IBR Control Logic

The per unit circuit diagram of the testbed is shown in Fig. 1. The hybrid power plant consists of a 100-MW GFL-IBR and a 100-MW GFM-IBR. The plant either operates in the grid-connected mode by connecting to the grid through a transformer or operates in the autonomous mode. The two IBRs are connected in parallel to the point of interconnection (POI) bus. The impedances between the POI bus and their PCC buses are assumed to be negligible.

The two IBR's converter control structures are shown in Fig. 2. IBR1 is the GFM type and IBR2 is the GFL type. In the GFL-IBR, the PLL-based synchronization, along with decoupled real and reactive power regulation through current vector control is deployed. In the GFM-IBR, the power-based synchronization is deployed and the inner current control is similar as that of the GFL. On the other hand, the outer controls that generate the current orders are quite different. This type of control structure has appeared in a 2007 paper [7] and a classic textbook [1] published in 2010. The outer controls have the goal to regulate dq voltage in the frame set up by the synchronizing angle. This synchronizing angle is generated by the power-frequency droop control. The dq voltage regulation is achieved by adjusting the shunt capacitor currents. Therefore, the outer voltage control generates the shunt capacitor's current orders. In order to generate the orders for the converter current, the output current exporting to the grid needs to be added. Therefore, two current sensors are needed, one for the converter current and the other for the output current. This control structure has been adopted popularly by the research community and is termed as multi-loop droop control [4].

Table I lists the parameters for the circuit and the controllers. The bandwidth of each control system has also been calibrated and presented in a column. Note that for PLL and GFM's outer voltage control, different sets of parameters will be examined for comparison.

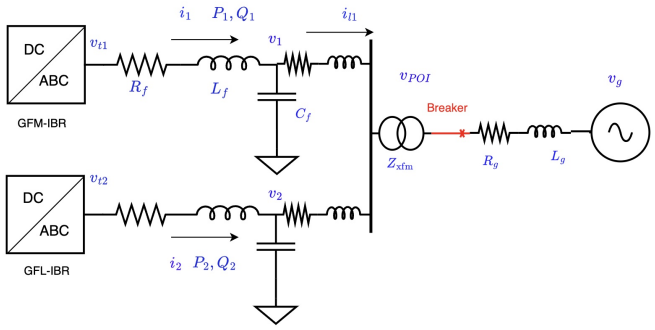

Fig. 1: Circuit topology of the testbed.

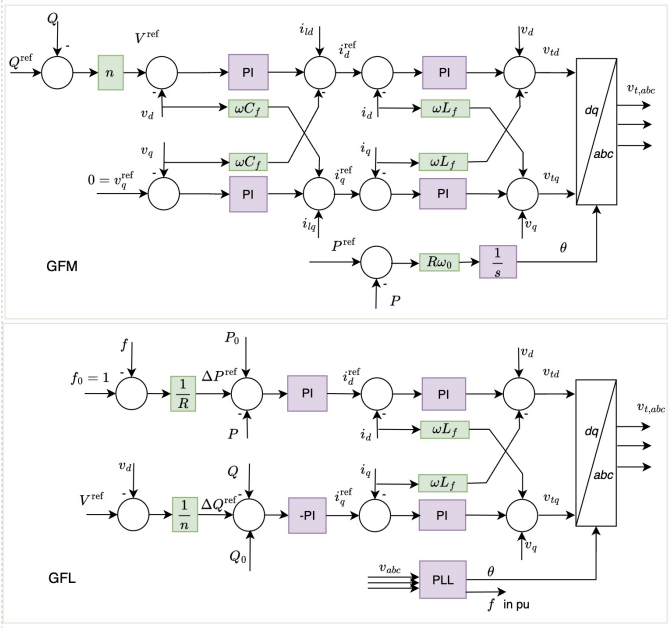

Fig. 2: GFM and GFL control block diagrams.

III. Small-Signal Stability: Strong Grid

It has been perceived by the research community that power-based GFM is vulnerable to small-signal stability issues when the grid strength is high. In this section, we illustrate the stability issues through two stages. In Stage 1, we examine the synchronizing feedback system for a GFM grid integrated system and explain why GFM-IBR is less stable in strong grids. In Stage 2, we further examine whether equipping GFL with frequency support can improve or deteriorate stability.

A. Stage 1: Single GFM system small-signal stability issue

It has been pointed out by the literature that while GFLs are less stable in weak grids [25], GFMs are opposite and they are less stable in strong grids [10]. In [10], the authors offer an explanation by assuming a GFM as a controllable voltage source and the synchronization is achieved through real current. The resulting synchronizing loop is a simplified version of a second-order system, as shown in Fig. 3. This synchronizing system has implicated that the open loop gain consists of an admittance, the real current to frequency droop,

TABLE I: Parameters for the circuit and the VSC control.

Description	Values (SI/pu)	bandwidth
Grid power base	200 MVA	
Grid reactance X_g	0.2 pu, 0.5 pu	
Grid resistance R_g	$0.1X_g$	
Transformer Z_{xfm}	$0.04 + j0.144$ pu	
IBR power base	100 MVA	
Choke filter R_f	0.001 pu	
Choke filter L_f	0.108 pu	
Shunt filter C_f	0.0803 pu	
GFM: P-f droop gain R_1	1% -15% pu/pu	
GFM: Q-V droop gain n_1	0.2	
GFL: f-P droop gain $1/R_2$	$10 - 100$ pu/pu	
GFL: PLL's PI controller	$60 + 1400/s$	13 Hz
	$180 + 3200/s$	32 Hz
Inner current control	$0.5 + 5/s$	278 Hz
GFL power control	$0.3 + 30/s$	4 Hz
GFL reactive power control	$0.3 + 30/s$	4 Hz
GFM voltage control	$2 + 2/s$	160 Hz
	$0.5 + 1/s$	60 Hz

and an integrator. Therefore, it can be reasoned that a small impedance or a strong grid may introduce instability.

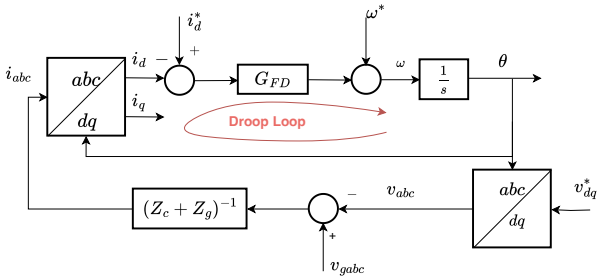

Fig. 3: The synchronizing loop based on Fig. 3a of [10]. Z_c stands for the IBR's impedance while Z_g stands for the grid impedance.

On the other hand, this simplified version has not included any characteristics associated with the rest of the control logic except the power-frequency droop control. In this research, we will fill the gap by including the GFM control characteristics into the synchronizing loop.

1) **GFM control design for angle tracking:** First, let's examine the power-frequency-angle feedback system for the GFM. The control design is very sophisticated involving both the inner and outer controls. Our interest is on the power-frequency-angle relationship. Therefore, we will form a simplified feedback system to facilitate our analysis. Note that the synchronizing angle is generated through the power-frequency droop control. At steady state, this angle aligns with the PCC bus voltage space vector's angle. This alignment is achieved through the q-axis outer-loop control where v_q is enforced to be 0.

Note that v_q is the PCC bus voltage space vector's projection on the synchronizing frame's q-axis, as shown in Fig. 4. Therefore, $v_q = \hat{v}\sin(\theta_{\text{PCC}} - \theta) \approx \theta_{\text{PCC}} - \theta$ (where θ_{PCC} is the angle of the PCC bus voltage space vector, while θ is the synchronizing angle). Additionally, $\hat{v}$ is assumed to be 1 pu during normal operation. It can be seen that enforcing the error to the PI controller $-v_q$ to be 0 is equivalent to enforce θ_{PCC} to track the synchronizing angle θ. The tracking speed is determined by the v_q control.

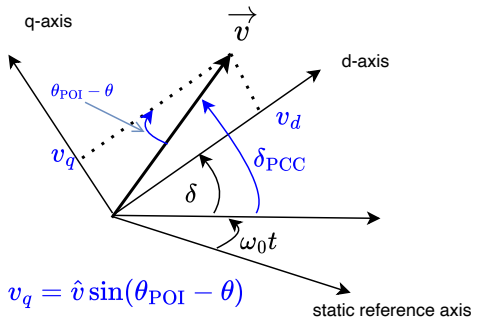

Fig. 4: Positions of the synchronizing frame, PCC bus voltage space vector.

Note that the outer control is based on a plant model of the shunt filter capacitor dynamics. The dq-axis outer control regulates the dq-axis voltage through PI controllers and adjusts the capacitor currents. If we bring the outer control's design into analysis, we can find that the closed-loop systems of dq-axis voltage regulation. From those closed-loop systems, how fast the PCC bus voltage angle tracks the synchronizing angle is known.

In the dq frame, the capacitor's dynamics can be written as:

$$C_f \frac{d\overline{V}}{dt} + j\omega C_f \overline{V} = \overline{I}_{\text{cap}}, \tag{1}$$

$$\implies C_f s v_d = \underbrace{i_{\text{cap,d}} + \omega C_f v_q}_{u_d}, \tag{2}$$

$$C_f s v_q = \underbrace{i_{\text{cap,q}} - \omega C_f v_d}_{u_q} \tag{3}$$

The plant model for voltage regulation is:

$$\frac{\Delta v_d}{\Delta u_d} = \frac{1}{C_f s}, \quad \frac{\Delta v_q}{\Delta u_q} = \frac{1}{C_f s} \tag{4}$$

The open-loop and closed-loop systems of the dq-axis voltage tracking system are as follows:

$$G_{OL}(s) = \left(K_p + \frac{K_i}{s}\right)\frac{1}{C_f s}\frac{1}{1+\tau s}, \tag{5}$$

$$G_A(s) = \frac{\Delta v_q}{\Delta v_q^*} \approx \frac{\Delta\theta_{\text{PCC}}}{\Delta\theta} = \frac{G_{OL}}{1+G_{OL}}, \tag{6}$$

where $1/(1+\tau s)$ represents the current tracking system as a low-pass filter (LPF). With the open-loop system consisting of two integrators, the closed-loop system $G_A(s)$ behaves as a LPF. It can be seen that the closed-loop system $G_A(s)$ represents Δv_q versus its reference signal. Since v_q represents the angle difference between the PCC bus angle θ_{PCC} and the synchronizing angle θ, v_q's dynamic response of returning to 0 is equivalent to the dynamic response of θ_{PCC} tracking θ.

The larger the PI controller's gains, the faster the closed-loop system responds. In other words, the angle tracking speed increases as the PI controller's parameters become larger.

In analysis, we check two different sets of PI parameters which lead to very different bandwidth of angle tracking. For $K_p = 1$, $K_i = 2$, $\tau = 0.02$ s, and $C_f = B_c/\omega_0$ where $B_c = 0.0803$ pu, the resulting bandwidth of the closed-loop

system $G(s)$ is 120 Hz. If the PI controller is $0.1 + 0.5/s$, the resulting bandwidth is about 37 Hz.

2) **Feedback system construction:** The v_q controller in the GFM enforces $-v_q$ or $\theta - \theta_{\rm PCC}$ to zero. This is similar as enforcing $\theta_{\rm PCC}$ to follow the synchronizing angle θ. Since the POI bus and the PCC bus are located very close, we may treat $\theta_{\rm PCC}$ and $\theta_{\rm POI}$ as the same. $\theta_{\rm POI}$ can be expressed as the sum of an angle with a constant frequency ω_0 and another angle $\delta_{\rm POI}$, which at steady state is a constant:

$$\theta = \omega_0 t + \delta,\ \ \theta_{\rm POI} = \omega_0 t + \delta_{\rm POI}.$$
$$\Longrightarrow \frac{\Delta\delta_{POI}}{\Delta\delta} = \frac{\Delta\theta_{\rm POI}}{\Delta\theta} = G_A(s). \tag{7}$$

Change in $\delta_{\rm POI}$ will influence the real power exporting from the GFM-IBR. Furthermore, the real power will influence δ through the P-f droop control. Therefore, we may form a feedback system describing the relationship, shown in Fig. 5.

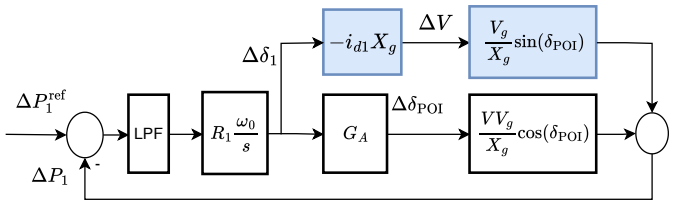

Fig. 5: The synchronizing feedback system for a GFM grid integration system. The LPF represents the low-pass filter used to smooth measurement signals.

The power measurement is compared with the power reference to generate an error, which is passed through a LPF for smoothing and further to the P-f droop control to generate the frequency deviation in pu. :

$$\Delta\omega = R_1(P_1^{\rm ref} - P_1), \tag{8}$$

where R_1 is the regulation parameter in the unit of pu/pu, and it is usually set in the range of 1% to 10%.

The frequency deviation in pu is multiplied by the nominal angular frequency ω_0 (377 rad/s) and integrated into the synchronizing angle δ_1 (rad). This synchronizing angle influences the POI angle through G_A or the v_q controller. The real power exported from the GFM-IBR to the grid is as follows:

$$P_1 = \frac{VV_g}{X_g}\sin(\delta_{\rm POI}),$$
$$\Longrightarrow \Delta P_1 = \frac{\Delta P_1}{\Delta\delta_{\rm POI}}\Delta\delta_{\rm POI} + \frac{\Delta P_1}{\Delta V}\Delta V, \tag{9}$$

where V_g is the grid's voltage and X_g is the grid impedance. It can be seen that

$$\frac{\Delta P_1}{\Delta\delta_{\rm POI}} = \frac{VV_g}{X_g}\cos(\delta_{\rm POI})$$
$$\frac{\Delta P_1}{\Delta V} = \frac{V_g}{X_g}\sin(\delta_{\rm POI}). \tag{10}$$

The P-f droop control, G_A and $\frac{\Delta P_1}{\Delta\delta_{\rm POI}}$ form the major loop in Fig. 5.

The blue blocks represent the effect of the GFM's synchronizing angle δ_1 on the PCC bus or POI bus voltage V, and further the effect of the voltage on the real power. It can be seen that if the GFM-IBR is assumed as a current source integrated to a purely reactive grid (the grid reactance notated as X_g), in a dq frame with a constant rotating speed of ω_0, which aligns with the POI voltage space vector at steady sate, this current source can be expressed as

$$\overline{I} = (i_d + ji_q)e^{j\delta}, \tag{11}$$

where δ is the synchronizing angle θ viewed in the synchronous rotating frame, and i_d and i_q are dq currents referred in the dq frame set up by the synchronizing angle. The angle difference between the synchronizing angle θ and the synchronous rotating frame is $\theta - \omega_0 t = \delta$.

Assuming that at the initial steady state, $\delta = \delta_{\rm POI} = 0$ and $i_q = 0$, then the small-signal expressions of the current phasor and further the POI voltage phasor are:

$$\Delta\overline{I} = \Delta i_d + ji_d\Delta\delta, \tag{12}$$
$$\Delta\overline{V} = jX_g\Delta\overline{I} = -i_dX_g\Delta\delta + jX_g\Delta i_d. \tag{13}$$

Since $\overline{V} = Ve^{j\delta_{\rm POI}}$, then

$$\Delta\overline{V} = \Delta V + jV\Delta\delta_{\rm POI}. \tag{14}$$

Therefore, $\Delta V = -i_dX_g\Delta\delta$. It can be seen that the synchronizing angle influences the voltage. Adding the impact of $\Delta\delta_1$ to ΔV and further to ΔP_1, the blue blocks are formed in Fig. 5.

If the effect of the synchronizing angle δ_1 on the PCC bus or the POI bus voltage V is ignored, the blue blocks can be ignored in Fig. 5. If this effect is included, it can be seen that the blue blocks act as a negative gain and decrease the total gain from the synchronizing angle $\Delta\delta_1$ to the real power ΔP_1. Therefore, it is expected that increasing the real current or power and/or increase the grid impedance can help stability.

Remark 1: The feedback system shown in Fig. 5 implicates that a large R_1 and a small X_g or a strong grid may introduce oscillation instability.

Remark 2: If we ignore the voltage's influence, the entire feedback system is very similar to a synchronous generator's swing dynamics. It can be seen if the transfer function from the POI angle to the synchronizing angle is a unit gain, the system is quite stable. Additionally, if the angle tracking speed is higher or v_q controller is fast, the system is more stable.

Remark 3: Increasing real power can help stability. The remarks will be verified through analysis EMT simulation results.

3) **Linear System Analysis Results:** We demonstrate the effect of grid strength X_g, the angle tracking control, and the GFM's P-f droop gain parameter R_1 on the GFM only system's small-signal stability. To make the feedback system simpler, the GFM is assuming to send out 0 real power and therefore the real current i_d is also 0. This eliminates the effect of the voltage variation on real power.

Fig. 6(a) shows the Bode diagrams of G_A (6), the transfer function from the synchronizing angle to the PCC bus voltage

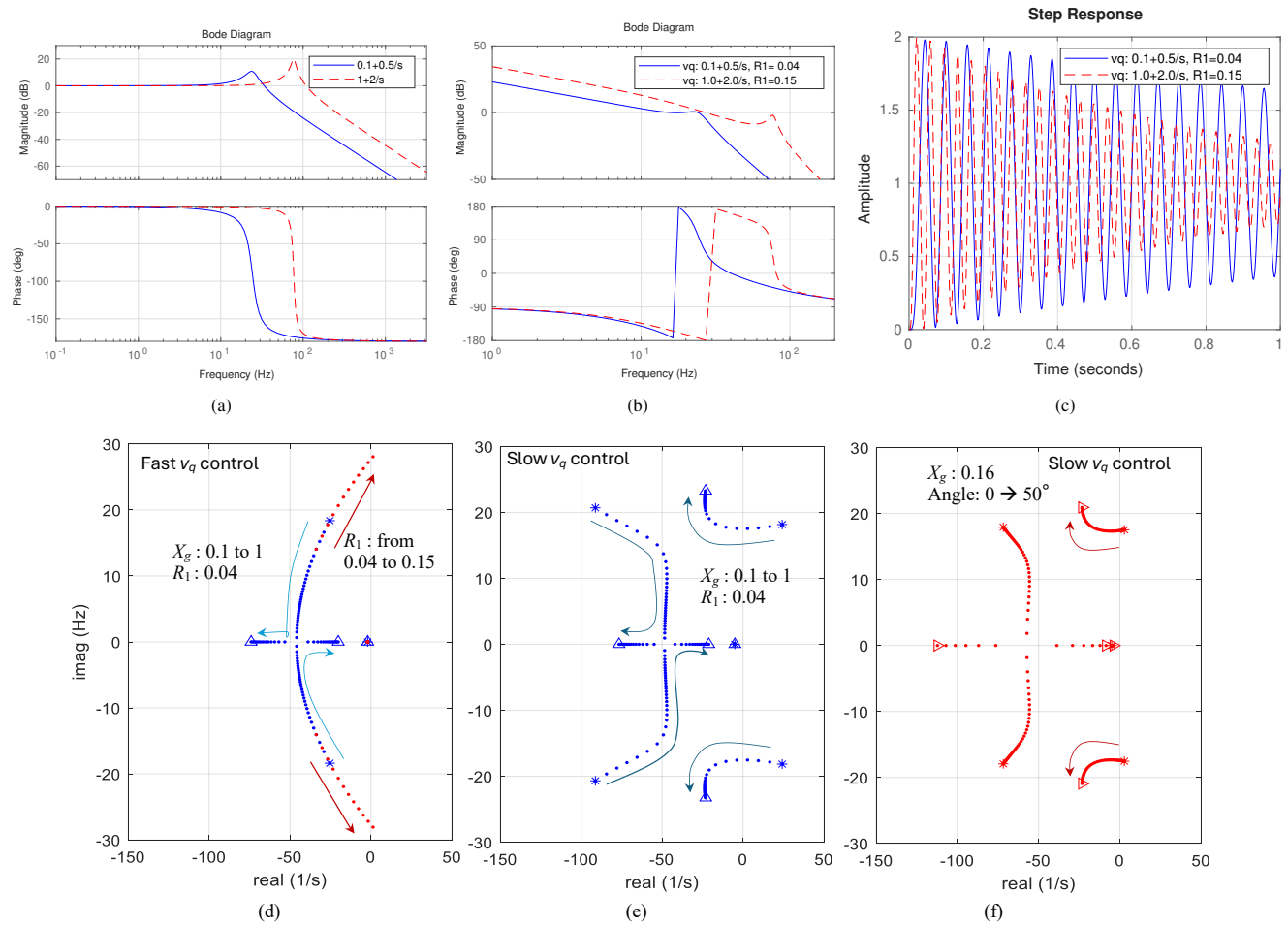

Fig. 6: Linear system analysis results. (a) The angle tracking system. 37 Hz bandwidth (slow) versus 120 Hz bandwidth (fast). (b) The open-loop system's Bode diagrams. R_1's gain: 0.04 or 0.15. (c) Step responses. In (a)-(c), the grid impedance is assumed as 0.17 pu. (d) Eigenvalues of the closed-loop system for the fast angle tracking control. (e) Eigenvalues of the closed-loop system for the slow angle tracking control. (f) Eigenvalues of the closed-loop system when the synchronizing angle varies from 0° to 50°.

phase angle. Two sets of the PI controller parameters are used to compare the performance of the system for a fast v_q controller and a slow v_q controller. The fast v_q control ensures a higher bandwidth of G_A and less phase lag in the subsynchronous region. In turn, the open-loop gain has its phase shifting frequency (when the phase angle changes from -180° to $+180^\circ$) delayed from about 15 Hz to 30 Hz, according to Fig. 6(b).

The analysis results in Fig. 6(b) of the open-loop gain of the system in Fig. 5 confirm that the open-loop gain's magnitude is proportionally related to the droop gain R_1 and $1/X_g$. A larger droop gain in a strong grid may introduce instability (Remark 1).

Furthermore, the oscillation's frequency is dependent on the v_q controller parameters (or the angle tracking control), as shown in both the open-loop gain Bode diagram in Fig. 6(b) and the step responses of the closed-loop systems in Fig. 6(c). A fast angle tracking control introduces less phase shift in the lower frequency region and therefore can accommodate a greater droop gain (shown in Fig. 6(b)). In this example, we show that for the slow angle control when the grid impedance is 0.17 pu, the droop gain cannot exceed 4%, while for the fast angle control, the droop gain can reach 15%. The analysis results confirm Remark 2 (fast voltage control is better for this type of oscillation stability).

The frequency-domain analysis method usually examines the open-loop gain's Bode diagrams, as shown in Fig. 6(b). The two Bode diagrams present two marginal stability cases for the slow and fast angle tracking control. In addition, eigenvalues can be computed based on the poles of the closed-loop system. In Fig. 6(d), the blue dots show the eigenvalue loci for the case of fast angle tracking control. When X_g changes from 0.1 to 1 or grid becomes weak, the dominant eigenvalue pairs move towards left. The system is always stable when X_g is in the range of $0.1-1$ and R_1 is 0.04. In addition, when X_g is fixed at 0.16 and R_1 increases from 0.04 to 0.15, the eigenvalues (red dots) move towards right. When R_1 reaches 0.15, the system is subject to oscillations close to 27 Hz.

As a comparison, Fig. 6(e) shows the eigenvalue loci for the slow angle tracking control. It can be seen that that the system is not always stable when X_g is in the range of 0.1–1 and R_1 is 0.04. Instead, X_g has to be greater than 0.16 for the system to be stable. Otherwise, the system is subject to

20-Hz oscillations.

Fig. 6(f) provides further analysis to show that when X_g is fixed at 0.16 and R_1 is fixed at 0.04, for the flow angle tracking control, if the synchronizing angle increases from 0° to 50°, the dominant oscillation mode will move to the left. This implies that higher power exporting from the GFM helps mitigate oscillations.

B. Stage 2: The effect of GFL's frequency support

In Stage 2, we consider the impact of the GFL when it is equipped with f-P control.

1) **Feedback system construction:** The feedback system has been updated to include GFL's f-P control effect, as shown n Fig. 7. The GFL's PLL tracks the PCC bus voltage phase angle, as shown in Fig. 7 (the yellow block). The block is the closed-loop transfer function of a PLL's angle tracking system and it acts as a low-pass filter:

$$\text{PLL} = \frac{\left(K_{p,\text{PLL}} + \frac{K_{i,\text{PLL}}}{s}\right)\frac{1}{s}}{1 + \left(K_{p,\text{PLL}} + \frac{K_{i,\text{PLL}}}{s}\right)\frac{1}{s}}. \tag{15}$$

The above closed-loop transfer function is for a simple second-order PLL with per unit voltage as input signals and it has been derived in many textbooks, including [1], [8]. For the PI control parameter set of (60,1400), this PLL leads to a bandwidth of 13 Hz (named as PLL1 in the following studies), for the parameter set of (180, 3200), this PLL leads to a bandwidth of 32 Hz (named as PLL2).

The PLL's output angle $\Delta\delta_2$ is used to generate a frequency for the f-P droop control. It can be seen that

$$\Delta P_2^{\text{ref}} = -\frac{1}{R_2}\frac{s}{\omega_0}\Delta\delta \tag{16}$$

where R_2 is the droop parameter in pu.

Furthermore, through the power PI controller, the power reference influences the d-axis' current order $\Delta i_{d2}^{\text{ref}}$ and further the d-axis current measurement Δi_{d2}. If the effect of voltage on real power is ignored, then $\Delta P_2 = V\Delta i_{d2} \approx \Delta i_{d2}$. Therefore the closed-loop system from the power reference to the power measurement can be expressed as follows:

$$G_P = \frac{\Delta P_2}{\Delta P_2^{\text{ref}}} = \frac{K_p + \frac{K_i}{s}}{1 + K_p + \frac{K_i}{s}} \tag{17}$$

For the PI controller of $0.30 + 30/s$, this is a low-pass filter of bandwidth 4 Hz.

It can be seen that the introduction of the f-P control influences the real power P_1, through the blocks in green. The total effect of the green blocks is equivalent to the addition of a high-pass filter. This addition can make stability worse.

2) **Linear System Analysis Results:** Fig. 8 shows the analysis results in three subplots. Fig. 8(a) shows the effect of the addition on the path from the synchronizing angle to the GFM's real power P_1. If there is no frequency support, the real power from the GFL P_2 can be viewed as constant. Therefore, $\Delta P_1 = \Delta P$, or the change in the total power from the plant to the grid is same as the change in P_1. With the GFL's frequency support, the synchronizing angle set up by the GFM's power-based synchronizing δ_1 now influences the GFL's PLL angle, which further influences the power order P_2^{ref}. So P_2 can no longer be assumed as constant. It can be seen that the effect of the GFL's frequency support acts as a high-pass filter. In the frequency range of 10 Hz, the GFL's frequency support makes the sensitivity from P_1 to δ_1 greater. In turn, the open-loop system's gain will be increased. This can lead to oscillation instability in that frequency range.

Fig. 8(b) further demonstrates the effect of the frequency support addition from the GFL on the overall feedback system. It can be seen that the addition makes the open-loop system gain greater and makes the previously stable system unstable. Finally, Fig. 8(c) shows the time-domain step responses of a change in P_1^{ref}. It can be seen that the oscillation stability becomes worse with the frequency support addition.

Fig. 9 shows the closed-loop system's eigenvalue loci for a changing R_2. The grid impedance and R_1 are fixed at 0.17 pu and 2.5%, respectfully. It can be seen that when $\frac{1}{R_2}$ increases, the dominant oscillation mode moves to the right. When $\frac{1}{R_2}$ becomes 40, the system is subject to marginal oscillatory stability. This set of analysis results again confirms that the GFL's frequency regulation may introduce unwanted interactions with the GFM. The greater $\frac{1}{R_2}$ (or the smaller R_2), the more unstable the system becomes. A smaller droop regulation parameter means that for the same frequency change, a generator is required to provide more power variation. This constraint on R_2's lower limit implies that the GFL's frequency support capability is limited in a hybrid power plant.

Remark 4: Introducing the f-P control in the GFL may worsen oscillation stability related to the synchronizing loop.

C. Verification of the remarks EMT simulation results

The EMT simulation results are shown in Figs. 10 and 12. The grid reactance is set as $X_g = 0.2$ pu for the power base of 200 MW. For the IBR's power base of 100 MW, this impedance is 0.1 pu. The grid strength is high. The GFM's outer controls are set as $0.5 + 1/s$ for both v_d and v_q control, while the GFL's outer controls are set as $0.30 + 30/s$ for real and reactive power regulation. The GFM's P-f droop gain is set to $R_1 = 0.02$, while the GFL's f-P gain is set as $1/R_2 = 80 = 1/0.0125$. Additionally, the Q-V droop gain n is set as 0.2.

Fig. 10 shows the simulation results when the Q-V droop is initially disabled and both IBRs send out 0 power. At $t = 0.5$ s, the power order of the GFM increases from 0 to 1. It can be seen that the synchronizing angle and the real power P_1 both increase. However, the system experiences 14-Hz oscillations. At $t = 1$ s, when the Q-V droop is enabled, the oscillations are dampened out. The Q-V droop control has the expression as follows:

$$\Delta V = -n\Delta Q \approx n\Delta i_q. \tag{18}$$

If we consider that voltage is around 1 pu, then $\Delta Q \approx -\Delta i_q$. n can be viewed as a reactance. Therefore, the V-Q droop control can be viewed as an equivalent circuit where a constant

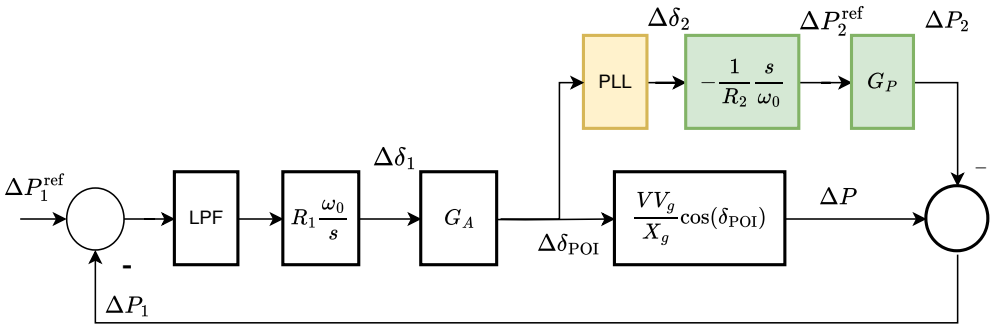

Fig. 7: The synchronizing feedback system for a GFM grid integration system.

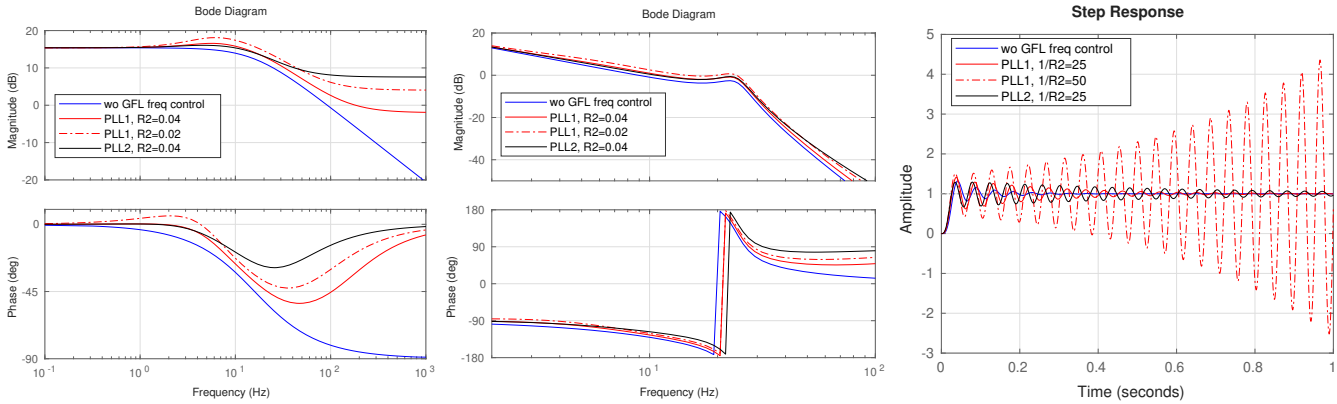

(a) (b) (c)

Fig. 8: The effect of adding frequency control in the GFL. GFM parameters: $R_1 = 0.025$, v_q controller: 37 Hz bandwidth. (a) Bode diagrams: from δ_1 to P_1. (b) The open-loop system. (c) Step responses of the closed-loop system from P_1^{ref} to P_1.

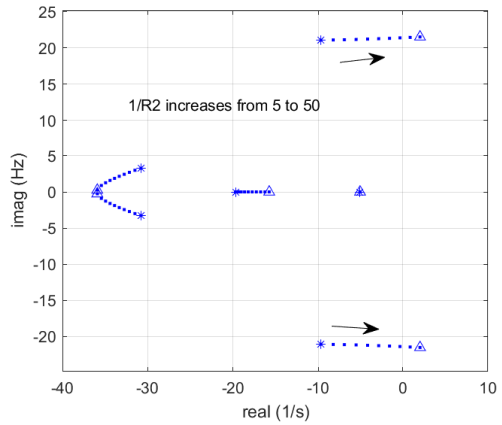

Fig. 9: Eigenvalue loci for a changing R_2. A larger $\frac{1}{R_2}$ or a small R_2 may introduce stability issue.

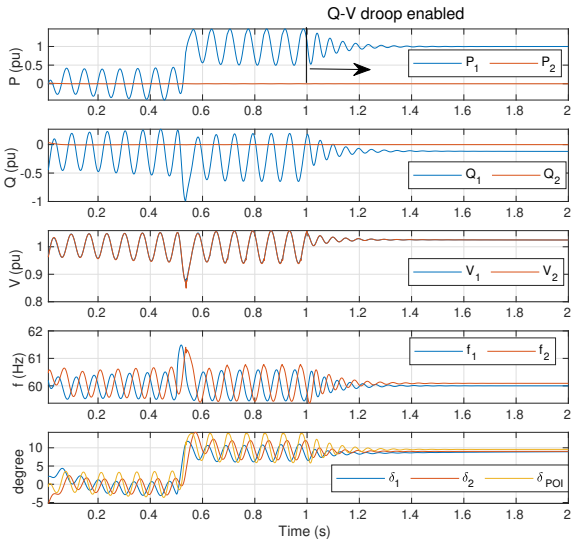

Fig. 10: The EMT simulation results. At $t = 1$ s, Q-V droop is enabled.

voltage source is behind a reactance with value of n, shown in Fig. 11. Equivalently, the V-Q control increases the effective grid impedance and thereby can enhance stability caused by the GFM's synchronizing system. This simulation result confirms Remark 1 that a larger grid impedance is beneficial or strong grid may introduce oscillations.

Fig. 12 shows the effect of real power exporting level, GFL's frequency control, and grid strength on stability. The Q-V droop is enabled for this study. Initially, the GFL's f-P

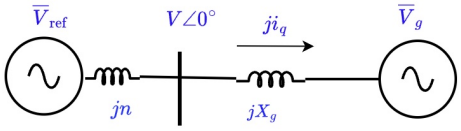

Fig. 11: The equivalent circuit of V-Q droop.

droop control is disabled. It can be seen that the system shows poorly-damped oscillations. At $t = 0.5$ s, the GFM's power order has a step change from 0 pu to 1 pu. It can be seen that the GFM real power measurement P_1 follows the order and also the system's oscillation damping enhanced. This confirms Remark 3 (increasing real power is beneficial to stability). At $t = 1$ s, the GFL's f-P droop control is enabled and the system is now subject to unstable 17-Hz oscillations. This confirms Remark 4 (the GFL's f-P control can make worsen stability). At $t = 1.5$ s, the grid strength reduces by doubling X_g. This helps oscillation damping. This again confirms Remark 1 (A large X_g is better for stability).

This case also compares a system without and with the GFL's frequency support. It can be seen that the addition can make stability worse. The EMT simulation results clearly show that the oscillations are most observable in GFM's real power and reactive power. The oscillations are visible in the GFL's real power and are negligible in reactive power. This fact implicates that the while the oscillations are largely associated with the GFM's control and the GFL's frequency support contributes to the oscillations as well. GFL's reactive power control does not contribute to the oscillations.

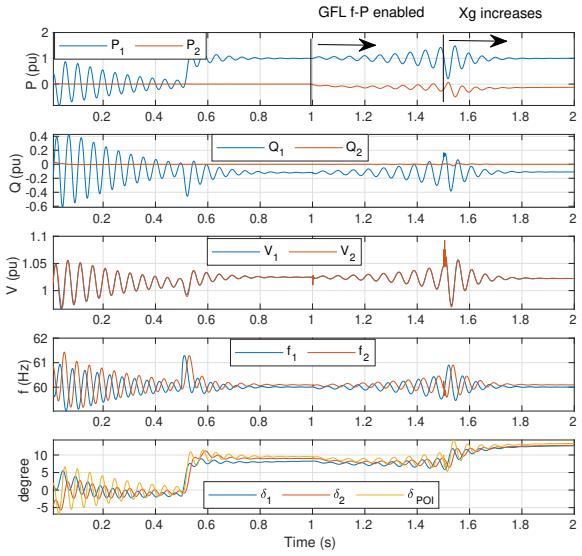

Fig. 12: The EMT simulation results. At $t = 0.5$ s, P_1^{ref} changes from 0 pu to 1 pu. At $t = 1$ s, the GFL's f-P control is enabled. It can be seen that oscillations appear. At $t = 1.5$ s, the grid strength reduces.

The stability issues can be resolved by having a faster voltage control. Fig. 13 shows the simulation results for the same set of events of Fig. 12. The voltage controller has a PI controller of $2 + 2/s$. It can be seen that the entire system works stably.

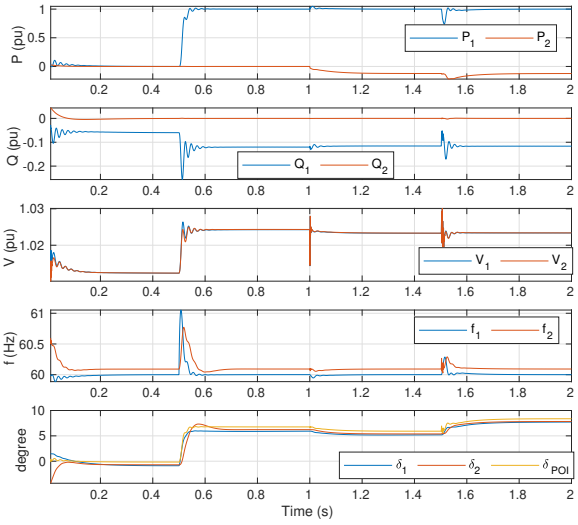

Fig. 13: The EMT simulation results for faster voltage control.

IV. Transient Stability Improvement through Additional Frequency Support

We illustrate the benefit of a well-designed GFM along with a GFL with frequency support. Frequency support is available in a GFM since it deploys power-based synchronization. This synchronization provides frequency support. When the system experiences frequency drop, the GFM will improve its output power. On the contrary, a GFL in the real power regulation control mode will not respond to frequency drop by improving its real power. Prior research has shown that adding frequency support can enhance synchronizing stability or suppress the large PLL angle increase for a grid voltage dip [26]. Large PLL angle deviation or PLL loss of synchronism has been observed in real world (2021 Texas Odessa disturbance) and resulted in large-scale solar PV tripping for a remote grid fault contingency [27]. Therefore, it is desirable to have not only GFM in a hybrid power plant but also equip the GFL-IBR with frequency support. The effect of the frequency control is demonstrated using EMT simulation.

Fig. 14 shows the EMT simulation results when the grid strength is about 2 pu for the 200 MW power base. The reactance of the grid is $X_g = 0.5$ pu. Initially, the IBR power plant is operating in the grid-connected mode. The two IBRs are exporting zero power. At $t = 1$ s, the GFM-IBR's power order P_1^{ref} increases from 0 pu to 1 pu (the power base is 100 MW). At $t = 2$ s, the GFL-IBR's power order P_2^{ref} increases from 0 pu and 1 pu. At $t = 3$ s, the grid voltage is subject to a 50% dip. This dip lasts for 0.05 s and the grid voltage recovers to 1 pu at 3.05s. At $t = 4$ s, the breaker between the transformer and the grid is open, disconnecting the power plant from the main grid.

The P-f droop gain R_1 for the GFM is 0.04 pu/pu (the power base is 100 MW), while the f-P gain for the GFL $1/R_2$ is 25 pu/pu (the power base is 100 MW). Therefore, both IBRs have the same f-P droop gain of 0.04. Before 4 s, both IBRs send out 1 pu real power. After 4 s, the main grid is disconnected

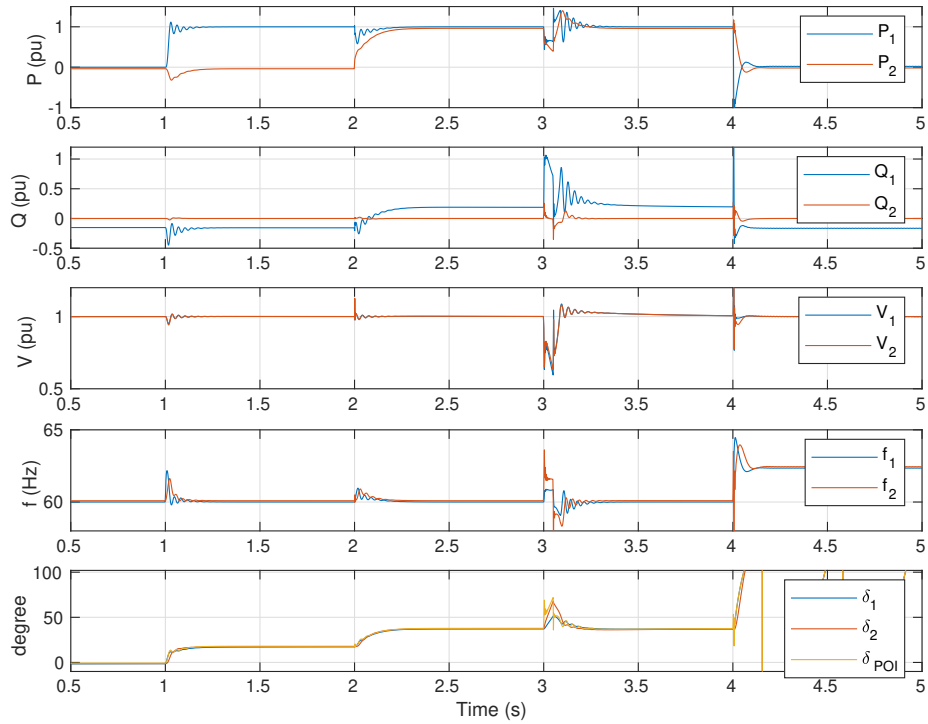

Fig. 14: EMT simulation results. At $t = 1$ s, the GFM's power order P_1^{ref} changes from 0 to 1 pu. At $t = 2$ s, the GFL's power order P_1^{ref} changes from 0 to 1 pu. From $3 - 3.05$ s, a voltage dip of 0.5 pu occurs at the grid voltage. At $t = 4$ s, the hybrid power plant is disconnected from the main grid.

and the IBRs serve 0 load power. Therefore, the total real power from the two IBRs should be 0 pu, implicating a drop of 2 pu real power. Based on the power-frequency relationship shown below:

$$\Delta P_1 = -\frac{1}{R_1}\Delta f, \;\; \Delta P_2 = -\frac{1}{R_2}\Delta f, \tag{19}$$

$$-2 = \Delta P_1 + \Delta P_2 = -\left(\frac{1}{R_1} + \frac{1}{R_2}\right)\Delta f \tag{20}$$

$$\Longrightarrow \Delta f = 0.04 \text{ pu} = 2.4 \text{ Hz}. \tag{21}$$

It can be seen that the frequency after disconnecting from the main grid should increase from 60 Hz to 62.4 Hz. This analysis result matches the final frequency shown in Fig. 15 at 5 s.

During the grid-connected operating condition (from the beginning to 4 s), the frequency is kept at 60 Hz at steady state despite disturbances. It can be seen that at $t = 1$ s, for a step change in the GFM's power order P_1^{ref}, the frequency f_1 immediately increases. This leads to the increase in the synchronizing angle δ_1. Increasing the synchronizing angle helps to increase the real power P_1 (when the voltage is kept relatively constant) to match its order eventually. On the other hand, from the control logic of the GFM, the increase in δ_1 leads to $v_q < 0$. Due to the cross coupling item from v_q to i_d^{ref} $(-B_{C_f} v_q)$, the real current order increases and this leads to the increase in real power until it matches the order. The v_q controller also responds to a dip in v_q. i_q^{ref} increases, which leads to the decrease in v_d. Due to the cross coupling unit $B_{C_f} v_d$ added to the i_q^{ref}, i_q^{ref} has to decrease. The two effects lead to oscillations in i_q^{ref} (and i_q) as well as Q_1. Therefore, Q_1 is seen to experience fast oscillations in the initial 0.2 seconds after the power order change.

The GFL's power order P_2^{ref} is based on the f-P droop control. When δ_1 increases, the POI angle δ_{POI} follows. Furthermore, the GFL's PLL angle δ_2 follows the POI angle. An increase in the angle leads to an increase in the frequency f_2. This further leads to the initial decrease in P_2 at $t = 1$ s due to the f-P droop control. Eventually P_2 is back to 0 pu and f_2 is back to 60 Hz.

At $t = 2$ s, the GFL's power order P_2^{ref} has a step change from 0 pu to 1 pu. In turn, the grid is subject to an increase in the real current injection. Consider an inductive transmission line:

$$\Delta v_d + j\Delta v_q = (\Delta i_d + j\Delta i_q) jX, \tag{22}$$

it can be seen that an increase in i_d leads to an increase in v_q. In the GFL IBR, the increase in v_q leads to the increase in the PLL's frequency f_2 and further the PLL's output angle δ_2. In the GFM IBR, the increase in v_q leads to the reduction in i_{q1}^{ref} due to the v_q controller and the decrease in i_{d1}^{ref} due to the cross coupling unit from v_q to the d-axis current order $(-B_{C_f} v_q)$. Therefore, the initial response after $t = 2$ s should be an increase in Q_1 and decrease in P_1. Eventually, P_1 is back to 1 pu to follow its order, P_2 also follows its oder and settles at 1 pu. The angles all settle at a larger value. Q_2 follows its order and settles at 0 pu while Q_1 increases to ensure the voltage at 1 pu.

At $t = 3$ s, the grid voltage is subject to a 50% dip and this

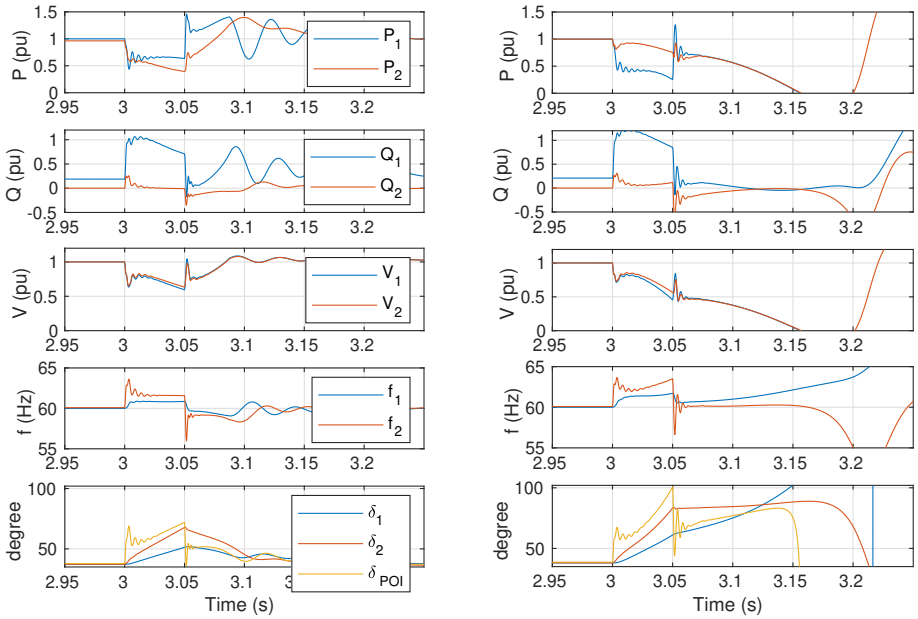

(a) (b)

Fig. 15: Comparison of with and without the frequency support from the GFL for a 0.5 pu voltage dip at the grid. (a) With the frequency support, the system is stable. (b) Without the frequency support, the system becomes unstable.

dip lasts for 0.05 s. The enlarged plots are shown in Fig. 15(a). For a side-by-side comparison, the simulation results for the case when the f-P droop control of the GFL is disabled are also presented in Fig. 15(b). It can be clearly seen that for a grid voltage dip, there is an immediate increase in the POI angle and an immediate decrease in the voltage. This translates to an increase in v_q and a decrease in v_d. The reason is that v_q is the projection of the POI voltage on the synchronizing frame and the synchronizing angle cannot change immediately, hence v_q has an immediate increase: $\Delta v_q > 0$. v_d also experiences an immediate decrease due to the grid voltage dip: $\Delta v_d < 0$. Based on the outer loop control logic, $\Delta v_q > 0$ leads to an immediate decrease in i_{d1}^{ref} due to the cross coupling item. Similarly, $\Delta v_d < 0$ leads to an immediate decrease in i_{q1}^{ref}. Compared to the effect of the cross-coupling items, the PI controllers act much slower. Therefore, the initial change can be seen as an increase in reactive power Q_1 and a decrease in real power P_1.

It can be seen that with the frequency support from the GFL, the GFL's real power decreases more since there is an increase in frequency due to voltage dip and the power order is reduced. Reduction in the real power helps boost voltage and also helps reduce the POI angle. Both benefit transient stability. The stabilizing effect of the frequency support can be clearly seen in Fig. 15.

V. Conclusion

In this paper, potential interactions among IBRs of two different types in a hybrid power plant have been demonstrated through EMT simulation studies. In addition, a set of feedback systems consisting of the frequency controls of GFL-IBR and GFM-IBR has been constructed. The block diagrams are used for quantitative stability analysis and identifying the influencing factors for stability. It is found that strong grid, a large P-f droop gain in the GFM, and introduction of additional frequency support in GFL, contribute to oscillations in the sub-synchronous region. It is also found that the voltage controller in the GFM should be tuned fast for smooth operation. In the power-angle feedback loop, fast control ensures fast angle tracking performance and reduces phase lag in the open-loop system. This characteristics helps oscillation stability. The learning from this research can help IBR coordination design and operation in a hybrid power system.

References

[1] A. Yazdani and R. Iravani, *Voltage-sourced converters in power systems: modeling, control, and applications*. John Wiley & Sons, 2010.

[2] I. S. Association *et al.*, "IEEE standard for interconnection and interoperability of inverter-based resources (IBRs) interconnecting with associated transmission electric power systems," *IEEE Std*, pp. 2800–2022, 2022.

[3] L. Zhang, L. Harnefors, and H.-P. Nee, "Power-synchronization control of grid-connected voltage-source converters," *IEEE Transactions on Power Systems*, vol. 25, no. 2, pp. 809–820, 2010.

[4] W. Du, Z. Chen, K. P. Schneider, R. H. Lasseter, S. Pushpak Nandanoori, F. K. Tuffner, and S. Kundu, "A comparative study of two widely used grid-forming droop controls on microgrid small-signal stability," *IEEE Journal of Emerging and Selected Topics in Power Electronics*, vol. 8, no. 2, pp. 963–975, 2020.

[5] P. Piagi and R. H. Lasseter, "Autonomous control of microgrids," in *2006 IEEE power engineering society general meeting*. IEEE, 2006, pp. 8–pp.

[6] Y. Li, D. Vilathgamuwa, and P. C. Loh, "Design, analysis, and real-time testing of a controller for multibus microgrid system," *IEEE Transactions on Power Electronics*, vol. 19, no. 5, pp. 1195–1204, 2004.

[7] N. Pogaku, M. Prodanovic, and T. C. Green, "Modeling, analysis and testing of autonomous operation of an inverter-based microgrid," *IEEE Transactions on power electronics*, vol. 22, no. 2, pp. 613–625, 2007.

[8] L. Fan and Z. Miao, *Modeling and Stability Analysis of Inverter-Based Resources*. CRC Press, 2023.

[9] H. Ding, R. Kar, Z. Miao, and L. Fan, "A novel design for switchable grid-following and grid-forming control," *IEEE Transactions on Sustainable Energy*, pp. 1–14, 2024.
[10] Y. Li, Y. Gu, and T. C. Green, "Revisiting grid-forming and grid-following inverters: A duality theory," *IEEE Transactions on Power Systems*, vol. 37, no. 6, pp. 4541–4554, 2022.
[11] Z. Zou, J. Tang, X. Wang, Z. Wang, W. Chen, G. Buticchi, and M. Liserre, "Modeling and control of a two-bus system with grid-forming and grid-following converters," *IEEE Journal of Emerging and Selected Topics in Power Electronics*, vol. 10, no. 6, pp. 7133–7149, 2022.
[12] X. He, S. Pan, and H. Geng, "Transient stability of hybrid power systems dominated by different types of grid-forming devices," *IEEE Transactions on Energy Conversion*, vol. 37, no. 2, pp. 868–879, 2022.
[13] Y. Wu, H. Wu, F. Zhao, Z. Li, and X. Wang, "Influence of PLL on stability of interconnected grid-forming and grid-following converters," *IEEE Transactions on Power Electronics*, vol. 39, no. 10, pp. 11 980–11 985, 2024.
[14] Y. Zhang, Y. Gu, Y. Zhu, T. C. Green, and H.-D. Chiang, "On the interaction in transient stability of two-inverter power systems containing gfl inverter using manifold method," *arXiv preprint arXiv:2501.05994*, 2025.
[15] E. A. Ducoin, Y. Gu, B. Chaudhuri, and T. C. Green, "Analytical design of contributions of grid-forming & grid-following inverters to frequency stability," *IEEE Transactions on Power Systems*, 2024.
[16] Y. Cheng, L. Fan, J. Rose, S.-H. Huang, J. Schmall, X. Wang, X. Xie, J. Shair, J. R. Ramamurthy, N. Modi, C. Li, C. Wang, S. Shah, B. Pal, Z. Miao, A. Isaacs, J. Mahseredjian, and J. Zhou, "Real-world subsynchronous oscillation events in power grids with high penetrations of inverter-based resources," *IEEE Transactions on Power Systems*, vol. 38, no. 1, pp. 316–330, 2023.
[17] R. Middlebrook, "Low-entropy expressions: the key to design-oriented analysis," in *Proceedings Frontiers in Education Twenty-First Annual Conference. Engineering Education in a New World Order*, 1991, pp. 399–403.
[18] R. D. Middlebrook, "Methods of design-oriented analysis: Low-entropy expressions," *New Approaches to Undergraduate Education IV*, 1992.
[19] F. P. Demello and C. Concordia, "Concepts of synchronous machine stability as affected by excitation control," *IEEE Transactions on Power Apparatus and Systems*, vol. PAS-88, no. 4, pp. 316–329, 1969.
[20] E. V. Larsen and D. A. Swann, "Applying power system stabilizers part i: General concepts," *IEEE Transactions on Power Apparatus and Systems*, vol. PAS-100, no. 6, pp. 3017–3024, 1981.
[21] H. Wu and X. Wang, "Design-oriented transient stability analysis of grid-connected converters with power synchronization control," *IEEE Transactions on Industrial Electronics*, vol. 66, no. 8, pp. 6473–6482, 2019.
[22] ——, "Design-oriented transient stability analysis of PLL-synchronized voltage-source converters," *IEEE Transactions on Power Electronics*, vol. 35, no. 4, pp. 3573–3589, 2020.
[23] G. Wu, H. Sun, X. Zhang, A. Egea-Àlvarez, B. Zhao, S. Xu, S. Wang, and X. Zhou, "Parameter design oriented analysis of the current control stability of the weak-grid-tied vsc," *IEEE Transactions on Power Delivery*, vol. 36, no. 3, pp. 1458–1470, 2021.
[24] L. Fan, Z. Miao, D. Ramasubramanian, Y. Cheng, N. Miller, and J. Fu, "Feedback and oscillations," *IEEE Power and Energy Magazine*, 2026.
[25] L. Fan, "Modeling type-4 wind in weak grids," *IEEE Transactions on Sustainable Energy*, vol. 10, no. 2, pp. 853–864, 2019.
[26] L. Fan, Z. Wang, and Z. Miao, "Large angle deviation in grid-following IBRs upon grid voltage dip," *IEEE Transactions on Energy Conversion*, 2023.
[27] Joint NERC and Texas RE Staff Report. (2021, September) Odessa Disturbance.

Lingling Fan (Fellow, IEEE) received the B.S. and M.S. degrees in electrical engineering from Southeast University, Nanjing, China, in 1994 and 1997, respectively, and the Ph.D. degree in electrical engineering from West Virginia University, Morgantown, in 2001.

Currently, she is a full professor with the University of South Florida, Tampa, where she has been since 2009. She was a Senior Engineer in the Transmission Asset Management Department, Midwest ISO, St. Paul, MN, form 2001 to 2007, and an Assistant Professor with North Dakota State University, Fargo, from 2007 to 2009. Her research interests include power systems and power electronics. Dr. Fan serves as Editor-in-Chief for IEEE Electrification Magazine and Associate Editor for IEEE trans. Energy Conversion.

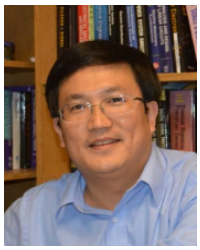

Zhixin Miao (Senior Member, IEEE) received the B.S.E.E. degree from the Huazhong University of Science and Technology,Wuhan, China, in 1992, the M.S.E.E. degree from the Graduate School, Nanjing Automation Research Institute (Nanjing, China) in 1997, and the Ph.D. degree in electrical engineering from West Virginia University, Morgantown, in 2002.

Currently, he is with the University of South Florida (USF), Tampa. Prior to joining USF in 2009, he was with the Transmission Asset Management Department with Midwest ISO, St. Paul, MN, from 2002 to 2009. His research interests include power system stability, microgrids, and renewable energy. Dr. Miao serves as an associate editor for IEEE trans. Sustainable Energy.

Deepak Ramasubramanian (Senior Member, IEEE) received the M.Tech. degree from the Indian Institute of Technology Delhi, New Delhi, India, in 2013 and Ph.D. degree at Arizona State University, Tempe, AZ, USA in 2017. Deepak is presently a Technical Leader in the Grid Operations and Planning Group at Electric Power Research Institute (EPRI) and leads research projects related to modeling of inverter-based resources for bulk power system analysis.